Available online at www.sciencedirect.com

SciVerse ScienceDirect

Ceramics International 39 (2013) 1153–1161

CERAMICS INTERNATIONAL

www.elsevier.com/locate/ceramint

ZrO_2 fibers obtained from the halide free synthesis of non-beaded PVA/Zr n-propoxide electrospun fibrous composites

Sarabjit Singh*, Vajinder Singh, M. Vijayakumar, V.V. Bhanu Prasad

Defence Metallurgical Research Laboratory, P.O. Kanchanbagh, Hyderabad 500058, India

Received 13 May 2012; received in revised form 19 June 2012; accepted 10 July 2012
Available online 3 August 2012

Abstract

The composite fibers of polyvinyl alcohol (PVA) and zirconium (Zr) n-propoxide were produced by an electrospinning process using the mixed solution of PVA and sol of zirconium n-propoxide. Effects of process parameters, viz. applied voltage, needle to collector distance and flow rate, were studied on the composite fibrous morphology. Bead-free composite fibers, with fiber diameter ranging from 155 nm to 850 nm, were produced with different process parameters. The morphology of the fibers varies significantly with the heat treatment. Heat treatment of the composite fibrous mats results in the removal of PVA, which causes the surface rough while retaining the fibrous morphology. The XRD studies reveal that the structure of PVA free ZrO_2 fibers is tetragonal.

Keywords: B. Electron microscopy; B. Fibers; D. ZrO_2

1. Introduction

Electrospinning has been proved to be the versatile technique to make ultrathin fibers with diameter down to nanometer range. Besides, this technique has gained much attention from both academicians as well as industrialists as it is simple and economical. The versatility of this low cost process for fiber making lies in its strength of producing fibers of polymers, metals, and ceramics as well as of composite systems [1–4]. Ultrathin fibers produced by this technique are enriched with the unique features such as high surface area, high surface area to volume ratio, small fiber diameter, prospective to incorporate active chemistry, filtration properties, high permeability and low weight which enable them for their application in various areas of biomedical applications (tissue engineering), sensor technology, filtration, super capacitors, catalysis, and optoelectronics [5–7].

The electrospinning technique involves application of high voltage to the tip of the syringe needle, filled with a polymeric solution, which deforms the solution droplet (coming out of the needle at a fixed flow rate) into a conical shape due to electrostatic repulsions between the surface charges as well as electrostatic attraction between the oppositely charged collector plates. When the applied voltage exceeds a threshold value, electrostatic forces overcome the surface tension and the ejection of a liquid jet from the orifice takes place. This is followed with a rapid bending and whipping process in which jet is continuously stretched and elongated by electrostatic repulsive forces, leading to the formation of a long, thin and uniform fiber. In this process, solvent rapidly evaporates and the fiber diameter reduces leading to the formation of an ultrathin fiber. Ultimately, the charged fibers deposit on the grounded collector plate as a result of electrostatic attraction. Bead free fibers with uniform diameters (throughout their length) can be produced after optimizing both the solution as well as process parameters. These parameters include surface tension, viscosity, needle to collector distance, applied voltage, flow rate and also ambient conditions like temperature and humidity [8–10].

Possibility of extending the concept of electrospinning to ceramic systems has opened a new era in nanoscale research during the past couple of years. Recently, numerous efforts have been made for the synthesis and characterization of

*Corresponding author. Tel.: +91 40 24586842; fax: +91 40 24340683.
E-mail addresses: sarabjit@dmrl.drdo.in, sarabdrdo@gmail.com (S. Singh).

0272-8842/$ - see front matter © 2012 Elsevier Ltd and Techna Group S.r.l. All rights reserved.
http://dx.doi.org/10.1016/j.ceramint.2012.07.039

ceramic fibers using electrospinning process for various applications. The typical materials include TiO_2, ZrO_2, Al_2O_3, Bi_2O_3, PZTs, PLZT, $BaTiO_3$ etc. [11–17]. The electrospun ceramic fibers are produced in the following steps: (i) preparation of electrospinning solution which includes stable sol of ceramic material and a carrier polymer to maintain the desired viscosity, (ii) electrospinning of the prepared solution and collection of the polymer/inorganic composite fibers/mat, (iii) heat-treatment of the composite fibers to remove unwanted constituents (polymer, solvent) and to obtain the desired ceramic phase and (iv) annealing for further modification of the fiber microstructure. Heat treatment is required to be done at a low heating rate in order to ensure the removal of organic components without destroying the fibrous morphology and also to avoid the disintegration of ceramic fibers.

This study presents synthesis of PVA/Zr n-propoxide fiber composite for ZrO_2 ceramic fibers. PVA (a carrier polymer) is generally used in the preparation of electrospun fibers of ceramic material because of its non-toxic nature, high water permeability, good film forming ability, high hydrophilicity, biocompatibility and good chemical and thermal stability [18–21]. ZrO_2 ceramics possess various valuable properties like high thermal and dimensional stability, high oxygen ion conductivity, low thermal conductivity together with relatively high coefficient of thermal expansion. These properties make this ceramic material useful as a catalyst/catalyst support for hydrogenation and isomerisation reactions compared with other ceramic oxides (TiO_2, SiO_2 and Al_2O_3), solid electrolytes in oxygen sensors and solid oxide fuel cells operating at lower temperatures, thermal barrier coating (TBC) applications and a ceramic biomaterial [22–24].

In literature, several efforts have been made to synthesize ultrafine zirconia fibers by the electrospinning process using poly(vinyl alcohol)/poly(vinyl pyrrolidone)/ethyl alcohol/distilled water/zirconium oxychloride composites as precursors followed by calcinations at various temperatures ranging from 600 °C to 1200 °C [13,25,26]. But the presence of halides like chloride ions have several disadvantages in terms of processing and device applications such as generation of corrosive HCl gas during the heat-treatment, requirement of inert atmosphere and inferior electronic property due to small amount of residual chloride [27,28]. Therefore, the present study is also focused on a halide free processing route for the preparation of zirconia fibers.

2. Experimental

Zirconium n-propoxide (analytical grade, Alfa-Aesar), poly(vinylalcohol) (PVA, Mw = 125,000 and degree of hydrolysis = 86–89%), acetyl acetone (Sigma Aldrich) and 2-methoxy ethanol (Sigma Aldrich), were used as starting materials in this work. PVA solution of 8 wt% was prepared by dissolving a weighed amount of PVA powder in deionized water at 85 °C with constant stirring. Precursor sol of Zr n-propoxide was prepared by the sol–gel technique as follows:

Zr n-propoxide was used as the precursor chemical for the synthesis of ZrO_2 fibers. Stabilization of Zr n-propoxide was achieved by the addition of acetyl acetone (chelating agent) in methoxy ethanol solvent. The molar ratio of acetyl acetone and Zr n-propoxide was kept 1:1. The basic mechanism for hydrolysis of $M(OR)_4$ has been given by Mazdiyasni et al. [29] as per the following reaction:-

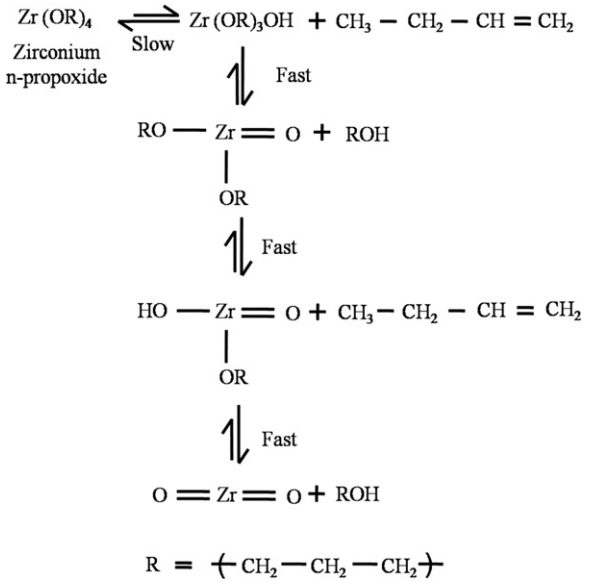

For zirconium alkoxides, hydrolysis is a much quicker reaction than condensation and hence, solid phase of ZrO_2 usually precipitates out before condensation. To slow down the hydrolysis, chelating agent was added to $Zr(OR)_4$, which produces the chelated complex as represented by the following reaction:-

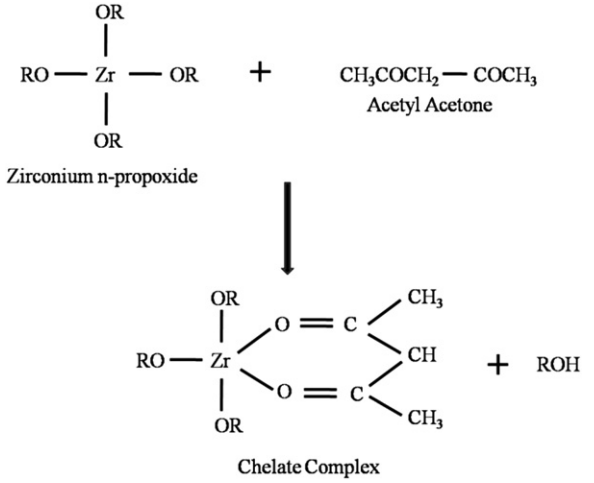

This chelated complex experiences much greater strain than the non-chelated one. As a result, they are least reactive towards hydrolysis and thus preventing the precipitation of ZrO_2.

Fibrous mats of PVA/Zr n-propoxide composite were prepared by using an Electrospinning (ES) setup manufactured by

TSPL Pvt. Ltd., Secunderabad, India which consists of a precisely programmable microprocessor based infusion syringe pump IP607 (five different grooves for using multiple syringes, capable of delivering flow rate of 0.2–200 μL/min), high voltage dc power supply (20 kV maximum voltage) and a collector plate. Collector plate covered with aluminum foil was kept at 90° to the needle to collect composite fibers. Both infusion syringe pump and collector plate were kept in a chamber, which has a wooden cabinet with a polycarbonate front window, LED bulbs and relays to indicate the running of the equipment and safety shut-off.

The syringe (capacity of 2 ml) was filled with a solution of PVA/ Zr n-propoxide composite solution (volume ratio of 4:1). To study the effect of process parameters (electric potential, collection distance and solution flow rate) on composite fiber morphology and diameters, fibrous mat structures of PVA/Zr n-propoxide composite were synthesized under following variable electrospinning conditions: voltage in the range of 7–11 kV, needle-to-collector distance in the range of 3.5–6.5 cm and flow rates in the range of 4.5–12.5 μL/min. All of these experiments were carried out on a stationary collector and for a fixed collection time of 1 min. A single fibrous mat was also deposited under one typical electrospinning condition, i.e. applied electrical potential of 13 kV with 8.5 μL/min flow rate over a fixed needle to collector distance of 4.5 cm and characterized from center to edge to study the changes in morphology and average diameter of composite submicron fibers. This deposition was done for 2 min.

As-deposited fibrous mat of PVA/Zr n-propoxide composite was heat-treated at 600 °C for 4 h in air using heating and cooling rates of 2 °C/min to produce polymer (PVA) free ZrO_2 fibers. The heat-treated as well as as-deposited sub-micron fibers were characterized by X-ray diffraction (XRD) and scanning electron microscope (SEM). The X-ray diffraction (XRD) of the samples were carried out in a Philips X-ray diffractometer using Cu Kα radiation with working current and voltage at 30 mA and 40 kV, respectively. Scans were made from 20° to 60° (2θ) at the speed of 2°/min and the step was 0.05°. The SEM images and EDS patterns of samples were recorded by using FEI Quanta 400 scanning electron microscope. Fiber diameter was determined from the SEM images of fibers using the UTHSCSA Image tool software. For each experimental condition, 50 different fibers were measured.

3. Results and discussions

3.1. Effect of needle–collector distance (NCD)

Fig. 1 shows the digital images, their corresponding SEM images and fiber diameter distribution of as prepared electrospun PVA/Zr n-propoxide fiber mat in the following conditions: applied voltage (13 kV), flow rate (8.5 μL/min.) and variable tip-to-collector distance (3.5–6.5 cm). The digital images also show that at the lowest distance, density of white portion i.e. the fibrous mat is very high and it decreases as the needle–collector distance increases. Decrease in the fiber density, i.e. number of fiber per unit area, is reflected in the corresponding SEM micrographs which showed the smaller fiber density for mat deposited at NCD of 6.5 cm. The plots of fiber size distribution show a shift in the fiber diameter distribution towards higher side. A narrow fiber size distribution was observed for NCD of 3.5 cm ranging between 170 nm and 550 nm. Composite fibrous mat showed a very high fiber size distribution ranging between 325 nm and 855 nm for NCD of 6.5 cm. Also, with the spread in distribution, the larger number of fibers within the distribution range shift towards the higher side (increasing fiber diameter).

The variation of average fiber diameter as a function of variable NCD is shown in Fig. 2. The plot shows the increase in fiber diameter with increase in needle–collector distance. With increase in the NCD, electric field strength decreases and a relatively less electrostatic repulsive force is experienced by the polymer jet which is being discharged. Due to this fact, jet velocity decreases resulting in less stretching of the polymer droplet coming out of the needle. Also, decrease in electrostatic force brings the bending instability close to the nozzle tip, causing an increase in the total path trajectory of the jet segment leading to increase in the diameters of the as-spun PVA/Zr n-propoxide composite fibers [30,31].

3.2. Effect of applied voltage

Digital images, their corresponding SEM images and fiber diameter distribution of as prepared electrospun PVA/Zr n-propoxide fiber mat have been shown in Fig. 3. The composite fiber mats were deposited under following electrospinning conditions: the variable applied voltage of 11–15 kV (in steps of 2 kV), the spinning solution flow rate 8.5 μL/min and the needle–collector distance (NCD) of 4.5 cm. It was observed that change in the applied voltage affects the diameters of the fibers and their size distribution. The diameter of the deposition area also decreases with increase in applied voltage. The fiber density increases with increasing the applied voltage and the most dense fiber mat was obtained for an applied maximum voltage of 15 kV. The increase in fiber density is also obvious from the SEM image of the corresponding digital picture. This behavior can be understood from the fact that the increase in electrostatic field strength increases the electrostatic force acting on a jet segment resulting in increase in the fiber density. Analysis of fiber size distribution plots reveals a broad size distribution of submicron fibers at 11 kV applied voltage and the spread of the size distribution reduces for 15 kV. The broad range distribution of fibers exists between 300 nm and 630 nm. When voltage is increased from 11 to 13 kV, the distribution of fiber diameter shifts towards the lower end and it exists between 230 and 550 nm. More narrow fiber size distribution (200–475 nm) was observed with further increase in the applied voltage to 15 kV. The effect of increasing the applied voltage can be realized as the

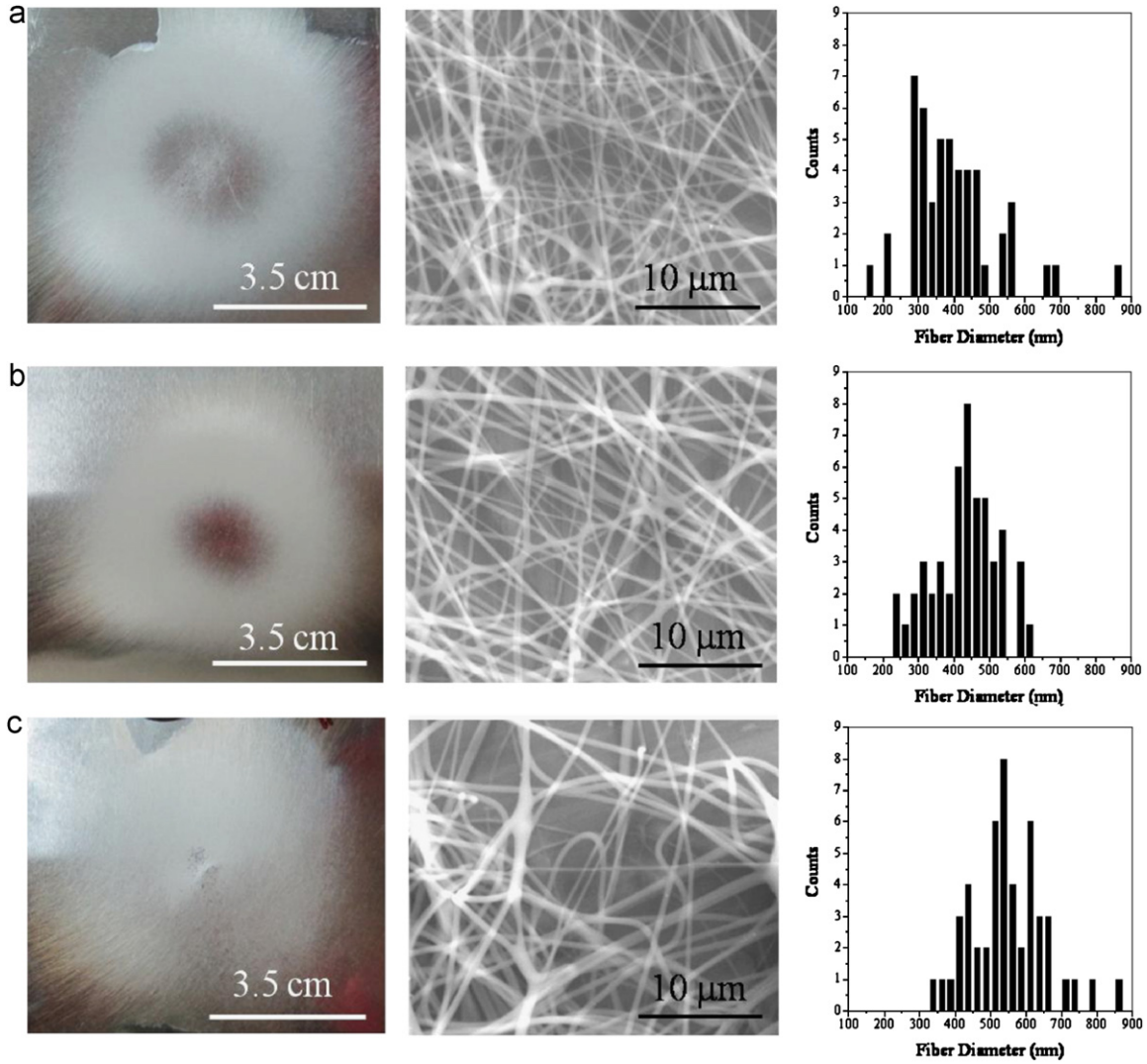

Fig. 1. Digital images of the deposition area, corresponding SEM images and size distribution of the as-spun PVA/Zr n-propoxide composite fibrous mats collected under the applied electric potential of 13 kV at fixed flow rate of 8.5 μl/min for three different NCDs: (a) 3.5 cm; (b) 4.5 cm and (c) 6.5 cm.

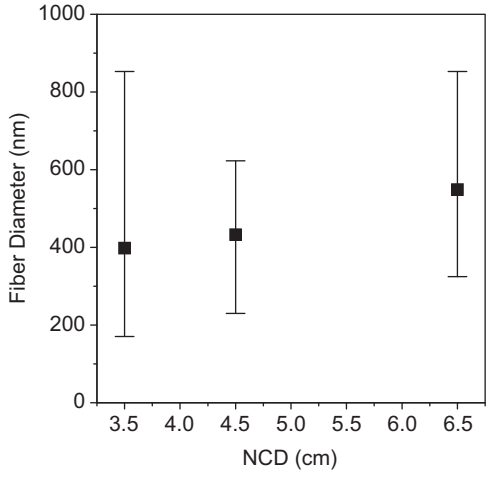

Fig. 2. Variation of average fiber diameter with NCD.

converse effect of decreasing the distance between needle and collector, thereby average fiber diameter showing the reverse trend.

The variation of average fiber diameter has been shown as a function of applied voltage in Fig. 4. It is found that average fiber diameter decreases with increase in the applied voltage; this is consistent with the earlier work reported in the literature [32–34]. The polymer droplet, which comes out of the tip of the needle at a fixed flow rate, experiences the large columbic forces as well as the stronger electric field with increase of applied voltage and during this exposure, the fibers face more stretching, therefore, reduction in the diameter takes place [35].

3.3. Effect of flow rate

Fig. 5 shows the digital images, their corresponding SEM images and fiber diameter distributions. To observe the effect of flow rate variation, electrospun PVA/Zr n-propoxide fiber mats were prepared under the following electrospinning conditions: applied electric potential (13 kV), needle-–collector distance (4.5 cm) and variable flow rates (4.5–12.5 μL/min). The digital images showed

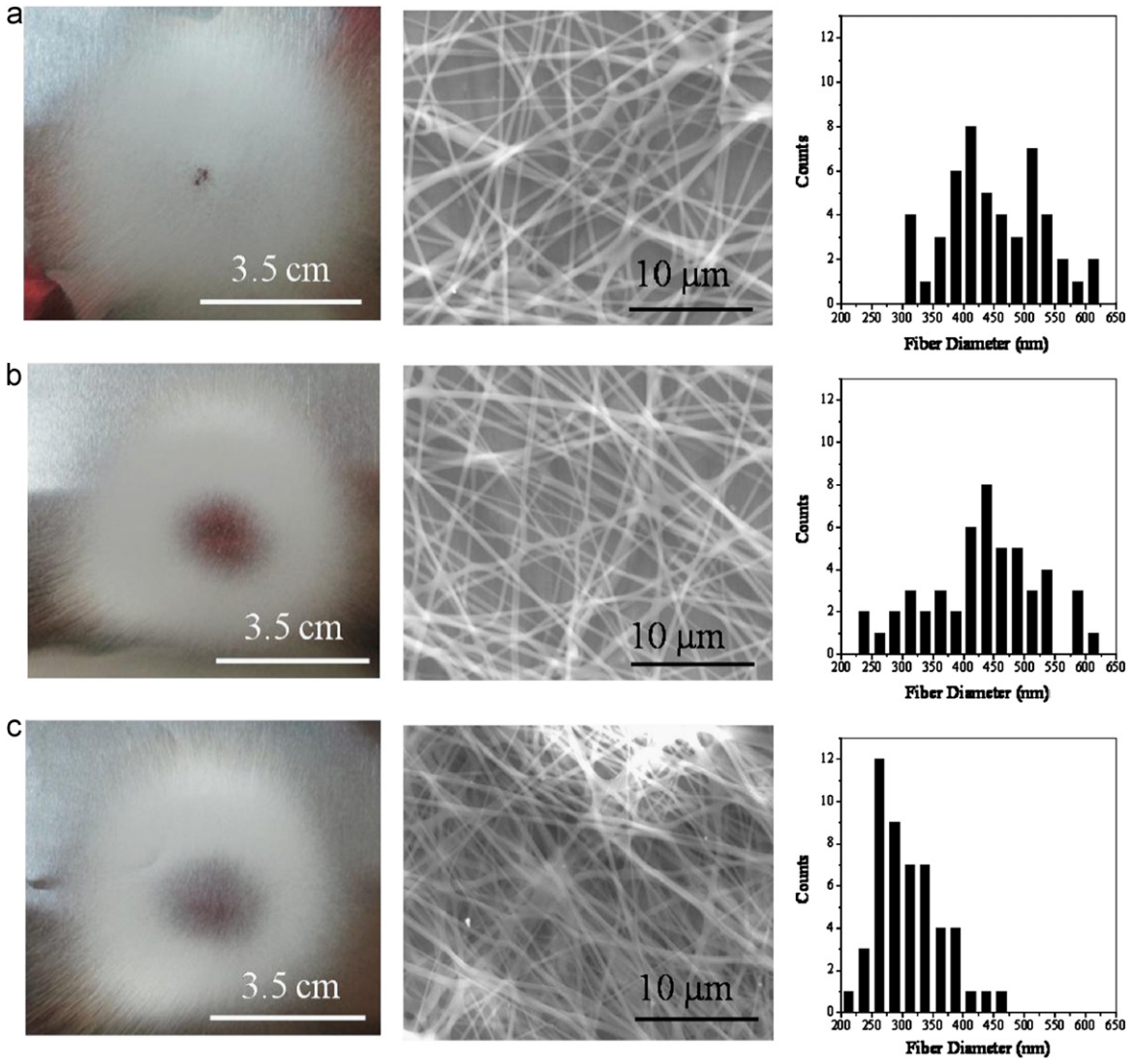

Fig. 3. Digital images of the deposition area, corresponding SEM images and size distribution of the as-spun PVA/Zr n-propoxide composite fibrous mats collected under different applied electric potentials of (a) 11 kV; (b) 13 kV and (c) 15 kV for a fixed NCD of 4.5 cm and a fixed flow rate of 8.5 μl/min.

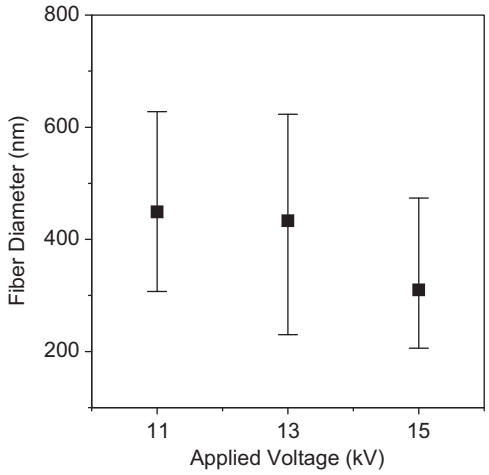

Fig. 4. Variation of average fiber diameter with applied voltage.

increase in fiber density with flow rate as reflected from the white portion (fibers) on the aluminum foil.

Fiber mat deposited with flow rate of 4.5 μL/min showed relatively small fiber density and this behavior is well supported by the SEM image for the same sample. The size distribution plots reveal that fiber size distribution shifts towards the lower side with an increase in flow rate. Also, a narrow size distribution was observed for relatively high flow rate of 12.5 μL/min. Maximum value of fiber diameter decreases from 725 nm to 465 nm with change in flow rate from 4.5 μL/min to 12.5 μL/min. From the SEM images, it is noticed that fiber concentration increases with increase in the flow rate and the most dense fibrous network was observed at highest flow rate of 12.5 μL/min.

Variation of average fiber diameter as a function of flow rate has been plotted in Fig. 6. The average fiber diameter showed first an increasing trend with increase in flow rate

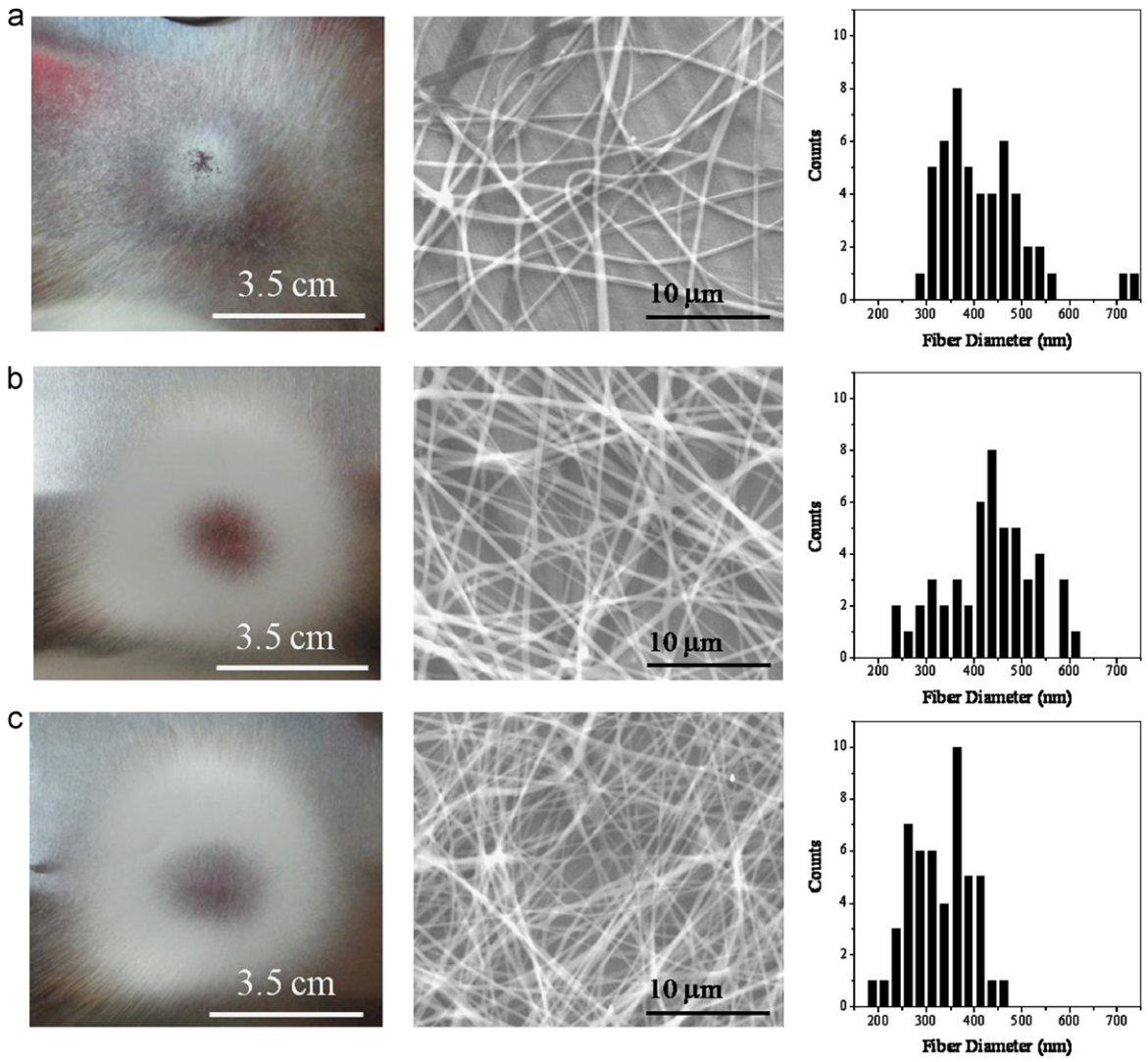

Fig. 5. Digital images of the deposition area, corresponding SEM images and size distribution of the as-spun PVA/Zr n-propoxide composite fibrous fiber mats collected under the applied electric potential of 13 kV at fixed collector distance of 4.5 cm for three different flow rates: (a) 4.5 μl/min; (b) 8.5 μl/min and (c) 12.5 μl/min.

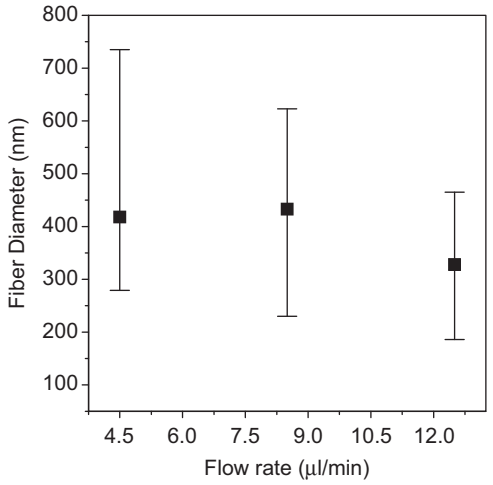

Fig. 6. Variation of average fiber diameter with flow rate.

up to 8.5 μL/min followed by a decrease in value for 12.5 μL/min. The average fiber diameter was found to be equal to 325 nm for the composite mat electrospun at 12.5 μL/min. The optimization of flow rate is very important in order to achieve bead-free electrospun fibers as the stable Taylor cone can be maintained for an optimized value of flow rate and applied voltage. With the increase in flow rate of the solution, larger volume of the polymer solution remains available which further gets drawn into the fibers, hence the solution carrying capacity of the jet increases and it carries with a relatively high velocity. Therefore, the time for the fibers to dry decreases and this leads to increase in the fiber diameter [36]. However, there is a limit to the increase in the diameter of the fiber due to higher feedrate. With further increase in the feed rate up to 12.5 μL/min, there is corresponding increase in the charges on the electrospinning jet which leads to corresponding increase in the stretching of the solution

and this aspect counters the increased fiber diameter due to increase in flow rate [37].

3.4. Morphological and structural analysis of ZrO_2 fibers obtained after heat-treatment of composite PVA/Zr n-propoxide fibers

To get PVA free pure ZrO_2 fibers, heat treatment of composite fibers was done at 600 °C for 4 h soaking time with 2 °C/min heating rate. The comparative microstructures have been given in Fig. 7(a and b) showing the difference in the morphology of as-spun composite PVA/Zr n-propoxide fibers and ZrO_2 fibers obtained after heat-treated respectively. The composite fibers were deposited under the electrospinning conditions of 11 kV applied voltage, 8.5 μL/min and 4.5 NCD. It was observed that heat-treated fibers show rough surface which is the effect of removal of polymer (PVA) from the composite fibers. After heat treatment, the average fiber diameter (AFD) was found to be 300 nm which is ~25% less than the AFD of composite fibers (435 nm). Also, most importantly, retainment of the fibrous morphology was observed after heat-treatment. The energy dispersive spectrum (EDS) of as-spun as well as heat-treated PVA/Zr n-propoxide composite fibers is reported in Fig. 7c and d, respectively. Peaks in the case of heat-treated fibers distinctly identify Zr and O as the elemental components which show the absence of organic content (no peak for carbon) confirming the formation of pure ZrO_2 fibers.

Fig.7e shows the XRD patterns of ZrO_2 fibers obtained by heat-treating the PVA/Zr n-propoxide composite fibrous mat. These fibers display the peaks corresponding to the tetragonal phase. The average size of crystallites was found to be equal to 8 nm.

3.5. Effect of distance from the center of as-spun PVA/Zr n-propoxide fiber mat

The microstructural details for a particular fibrous mat, deposited at electrospinning conditions of 13 kV applied voltage, 4.5 cm NCD and 8.5 μL/min flow rate, have been shown in Fig. 8. Four different equally distant positions in the as-spun composite fibrous mat were chosen (along with line marked as 1, 2, 3 and 4) for systematic investigation of the effect of distance from the center of mat to its edge on the

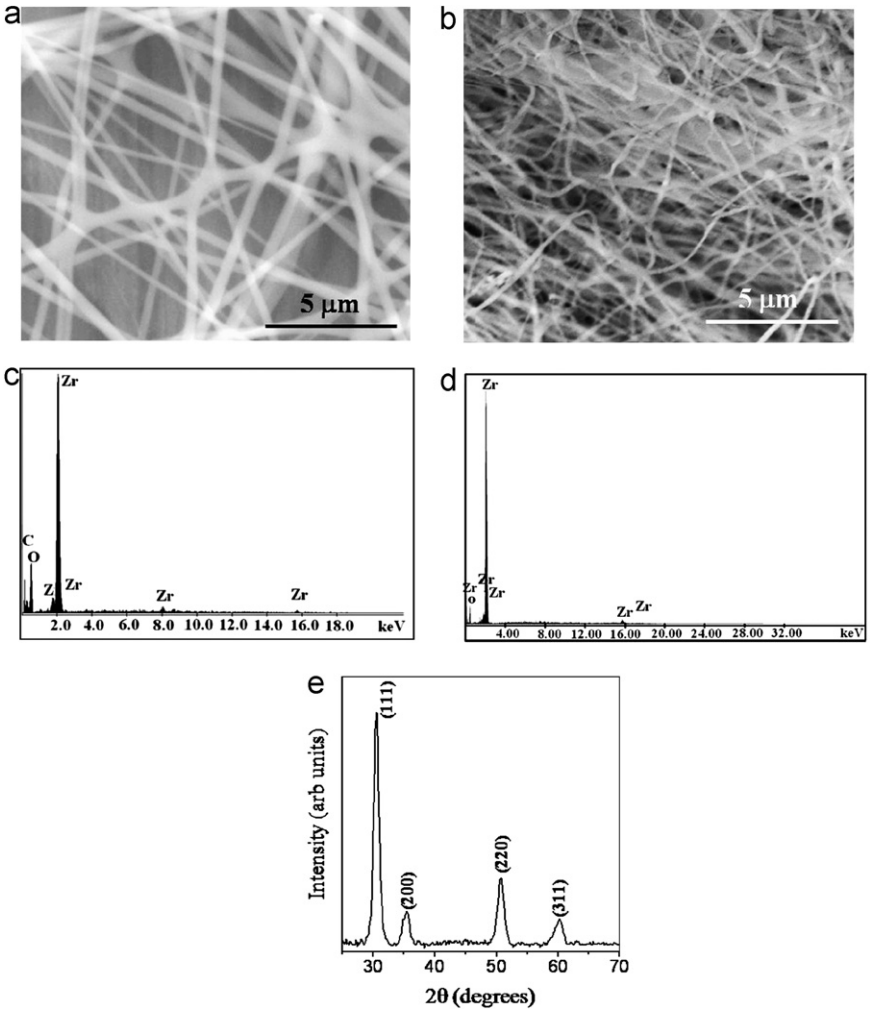

Fig. 7. SEM image of (a) as-spun and (b) heat-treated PVA/Zr n-propoxide composite fibrous mat; EDS patterns of (c) as-spun and (d) heat-treated PVA/Zr n-propoxide composite fibrous mat; (e) X-ray diffraction spectra for ZrO_2 fibers.

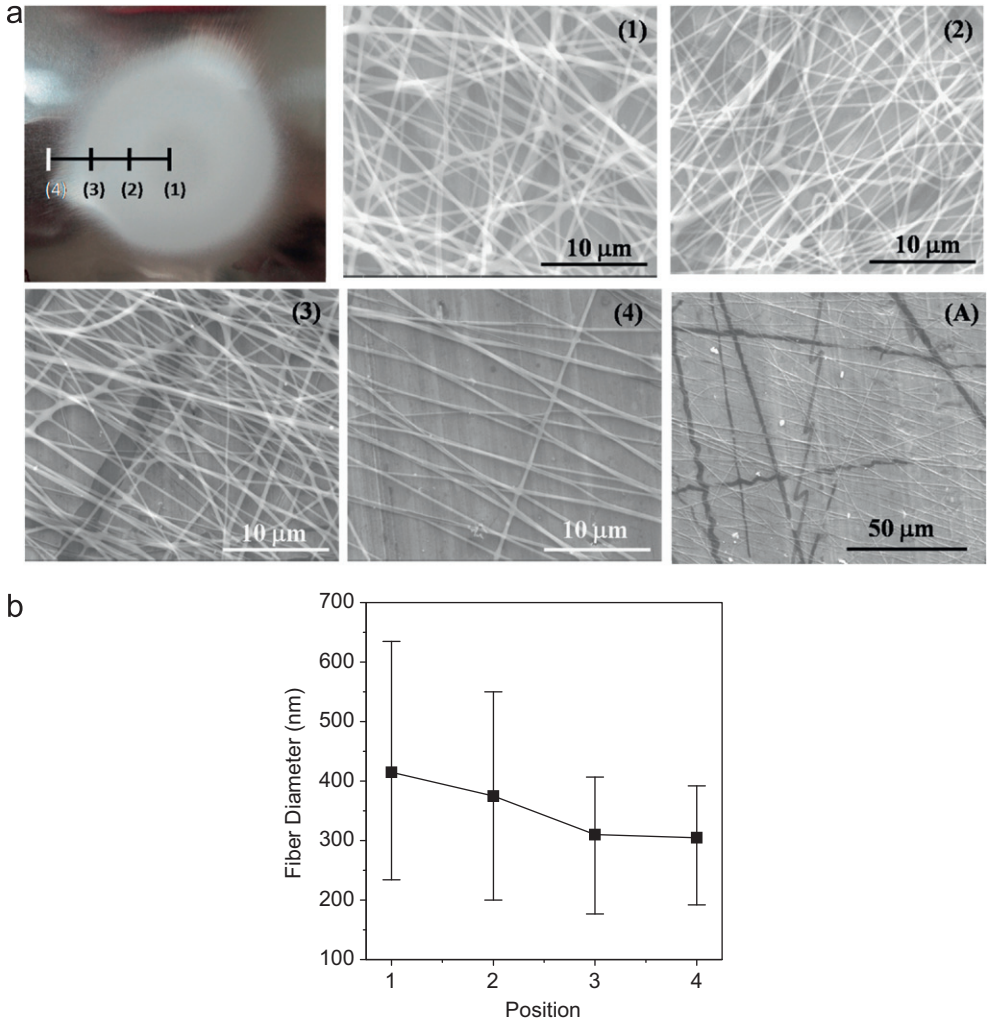

Fig. 8. (a) Digital image as well as corresponding SEM images at four different positions (1, 2, 3 and 4) and (b) variation of average fiber diameter as a function of distance variation from center to edge.

morphology and diameter of the fibers. Three major observations made from the SEM studies are: (i) decrease in average fiber diameter from center (418 nm) to edge (308 nm) (Fig. 8b); (ii) bead-free fibers throughout the distance and (iii) decrease in fiber density from center to edge region of the fibrous mat. Fibers are also uniform in diameter throughout their length irrespective of center or edge. Fiber diameter distribution was found to decrease with increase in distance from the center of the mat to its edge. Also, interestingly, fibers at the edge possess more stretching behavior as compared to those at the center; this results in their straightening effect up to some micron distance as it can be seen from the SEM micrograph [(A)] (at lower magnification).

4. Conclusions

Effect of process parameters of the electrospinning on the structure and morphology of fibers was explored for the first time on the chloride free preparation route of PVA/Zr n-propoxide composite fibrous mats obtained by using the direct sol of zirconium n-propoxide. It was observed that bead-free composite fibers show a significant variation in their average diameters as well as diameter range for all the three process parameters. Average fiber diameter increases with increase in NCD and decreases with increase in applied voltage whereas the dual behavior was observed for increase in flow rate of the electrospinning solution. Heat-treated composite fibers resulted in pure ZrO_2 fibers with tetragonal structure and ~25% reduction in the average diameter and also, most noticeably, without the loss of fibrous characteristics. The average crystallite size was found to be equal to 8 nm. A systematic study to see the change in microstructure from center to edge of as-spun PVA/Zr n-propoxide fibrous mat revealed bead-free fibers (throughout the distance) and also straight fiber morphology at the edge as compared to the center.

Acknowledgments

Authors gratefully acknowledge Dr. G. Malakondaiah, Director, Defence Metallurgical Research Laboratory (DMRL), Hyderabad for giving permission to publish the

work. Authors would also like to thank Dr. P. Ghosal, Scientist, DMRL, Hyderabad for providing the access of SEM facility besides the regular schedule and Dr. Subir Roy, Scientist, DMRL, Hyderabad for helping in the sol preparation.

References

[1] D.H. Reneker, I. Chun, Nanometer diameter fibers of polymer, produced by electrospinning, Nanotechnology 7 (1996) 216–223.
[2] X. Zong, K.S. Kim, D. Fang, S. Ran, B.S. Hsiao, B. Chu, Structure and process relationship of electrospun bioabsorbable nanofiber membranes, Polymer 43 (2002) 4403–4412.
[3] K. Ma, C.K. Chan, S. Liao, Y.K. William, Q. Feng, S. Ramakrishna, The influence of electrospun aligned poly(ε-caprolactone)/collagen nanofiber meshes on the formation of self-aligned skeletal muscle myotubes, Biomaterials 29 (2008) 2899–2906.
[4] G. Renuga, K. Satinderpal, Y.F. Chao, C. Casey, R. Seeram, Electrospun nanofibrous polysulfone membranes as pre-filters: particulate removal, Journal of Membrane Science 289 (2007) 210–219.
[5] H. Yoshimoto, Y.M. Shin, H. Rerai, J.P. Jin, H.J. Cacanti, A biodegradable nanofiber scaffold by electrospinning and its potential for bone tissue engineering, Biomaterials 24 (2003) 2077–2082.
[6] X. Wang, C. Drew, S.H. Lee, K.J. Senecal, Electrospun nanofibrous membranes for highly sensitive optical sensors, Nano Letters 2 (2002) 1273–1275.
[7] X. Lu, C. Wang, Y. Wei, One-dimensional composite nanomaterials: synthesis by electrospinning and their applications, Small 5 (2009) 2349–2370.
[8] D. Li, Y. Xia, Electrospinning of nanofibers: reinventing the wheel, Advanced Materials 16 (2004) 1151–1170.
[9] Z.M. Huang, Y.Z. Zhang, M. Kotaki, S. Ramakrishna, A review on polymer nanofibers by electrospinning and their applications in nanocomposites, Composites Science and Technology 63 (2003) 2223–2253.
[10] K. Jayaraman, M. Kotaki, Y. Zhang, X. Mo, S. Ramakrishna, Recent advances in polymer nanofibers, Journal of Nanoscience and Nanotechnology 4 (2004) 52–65.
[11] Y. Junhan, P. Louis, M.W. Sigmund, C.N. Juan, Electrospinning of complex oxide nanofibers, Physica E 37 (2007) 254–259.
[12] C. Wang, C. Shao, L. Wang, L. Zhang, X. Li, Y. Liu, Electrospinning preparation, characterization and photocatalytic properties of Bi_2O_3 nanofibers, Journal of Colloidal and Interface Science 333 (2009) 242–248.
[13] C. Shao, H. Guan, Y. Liu, J. Gong, N. Yu, X. Yang, ZrO_2 nanofibres via an electrospinning technique, Journal of Crystal Growth 267 (2004) 380–384.
[14] S. Xu, Y. Shi, S.G. Kim, Fabrication and mechanical property of nano piezoelectric fibers, Nanotechnology 17 (2006) 4497–4501.
[15] N. Dharmaraj, C.H. Kim, H.Y. Kim, Pb(Zr0.5, Ti0.5)O_3 nanofibres by electrospinning, Materials Letters 59 (2005) 3085–3089.
[16] Y. Zhao, H. Wang, X. Lu, X. Li, Y. Yang, C. Wang, Fabrication of refining mesoporous silica nanofibers via electrospinning, Materials Letters 62 (2008) 143–146.
[17] S. Singh, S. Roy, V. Singh, M. Vijayakumar, Synthesis and morphology of electrospun PVA/PLZT composite and single phase PLZT nanofibers, Materials Science and Engineering B 176 (2011) 1099–1109.
[18] C. Shao, H.Y. Kim, J. Gong, B. Ding, D.R. Lee, S. Park, Fiber mats of poly(vinyl alcohol)/silica composite via electrospinning, Journal of Material Science Letters 57 (2003) 1579–1584.
[19] M. Krumova, D. López, R. Benavente, C. Mijangos, J.M. Pereña, Effect of crosslinking on the mechanical and thermal properties of poly(vinyl alcohol), Polymer 41 (2000) 9265–9272.
[20] R.M. Hodge, G.H. Edward, G.P. Simon, Water absorption and states of water in semisrystalline poly(vinyl alcohol) films, Polymer 37 (1996) 1371–1376.
[21] X.H. Qin, S.Y. Wang, Filtration properties of electrospinning nanofibers, Journal of Applied Polymer Science 102 (2006) 1285–1290.
[22] T. Yamaguchi, Zirconium in catalysis. Application of ZrO_2 as a catalyst and a catalyst support, Catalysis Today 20 (1994) 199–217.
[23] P. Charpentier, P. Fragnaud, D.M. Schleich, E. Gehain, Preparation of thin film SOFCs working at reduced temperature, Solid State Ionics 135 (2000) 373–377.
[24] D.R. Clarke, C.G. Levi, Materials design for the next generation thermal barrier coatings, Annual Review of Materials Research 33 (2003) 383–417.
[25] H.B. Zhang, M.J. Edirisinghew, Electrospinning zirconia fibre from a suspension, Journal of the American Ceramic Society 89 (2006) 1870–1875.
[26] N. Jing, M. Wang, J. Kameoka, Fabrication of ultrathin and uniform ZrO_2 nanofibers by electrospinning, Journal of Photopolymer Science and Technology 18 (2005) 503–506.
[27] G. Pfaff, A novel reaction path to barium zirconates by the decomposition of peroxide precursors, Materials Letters 24 (1995) 393–397.
[28] G. Pfaff, Synthesis of magnesium stannates by thermal decomposition of peroxo precursors, Thermochimica Acta 237 (1994) 83–90.
[29] K.S. Mazdiyasni, C.T. Lynch, J.S. Smith, Preparation of ultra-high-purity submicron oxides, Journal of the American Ceramic Society 48 (1965) 372–375.
[30] F.R. Lamastra, A. Bianco, A. Meriggi, G. Montesperelli, F. Nanni, G. Gusmano, Nanohybrid PVA/ZrO_2 and PVA/Al_2O_3 electrospun mats, Chemical Engineering Journal 145 (2008) 169–175.
[31] Y.C. Ahn, S.K. Park, G.T. Kim, Y.J. Hwang, C.G. Lee, H.S. Shin, J.K. Lee, Development of high efficiency nanofilters made of nanofibers, Current Applied Physics 6 (2006) 1030–1035.
[32] J.S. Lee, K.H. Choi, H.D. Ghim, S.S. Kim, D.H. Chun, H.Y. Kim, W.S. Lyoo, Role of molecular weight of atactic Poly(vinyl alcohol) (PVA) in the structure and properties of PVA nanofabric prepared by electrospinning, Journal of Applied Polymer Science 93 (2004) 1638–1646.
[33] S. Megelski, J.S. Stephens, D.B. Chase, J.F. Rabolt, Micro- and nanostructured surface morphology on electrospun polymer fibers, Macromolecules 35 (2002) 8456–8466.
[34] K.J. Pawlowski, H.L. Belvin, D.L. Raney, J. Su, J.S. Harrison, E.J. Siochi, Electrospinning of a micro-air vehicle wing skin, Polymer 44 (2003) 1309–1314.
[35] J.M. Deitzel, J. Kleinmeyer, D. Harris, N.C.B. Tan, The effect of processing of electrospun nanofibers and textiles, Polymer 42 (2001) 261–272.
[36] X.H. Zhong, K.S. Kim, D.F. Fang, S.F. Ran, B.S. Hsiao, B. Chu, Structure and process relationship of electrospun bioabsorbable nanofiber membranes, Polymer 43 (2002) 4403–4412.
[37] G.C. Rutledge, Y. Li, S. Fridrikh, S.B. Warner, V.E. Kalayci, P. Patra, Electrostatic Spinning and Properties of Ultrafine Fibers, Annual Report (M98-D01), National Textile Center, 2001, p. 1.